Disulfide Bonds in the Outer Layer of Keratin Fibers Confer Higher Mechanical Rigidity: Correlative Nano-Indentation and Elasticity Measurement with an AFM[†]

Ashok N. Parbhu,*[,‡,§] Warren G. Bryson,[‡] and Ratneshwar Lal*[,§]

Neuroscience Research Institute, University of California Santa Barbara, California 93106 and Wool Research Organization of New Zealand, Christchurch, New Zealand

Received March 31, 1999; Revised Manuscript Received June 29, 1999

ABSTRACT: Nanomechanical properties of biological fibers are governed by the morphological features and chemically heterogeneous constituent subunits. However, very little experimental data exist for nanoscale correlation between heterogeneous subunits and their mechanical properties. We have used keratin-rich wool fibers as a model of composite biological fibers; a wool fiber is a simple two component cylindrical system consisting of a core cellular component surrounded by an outer cell layer and their ultrastructure and chemical composition are well-characterized. The core is 16−40 μm in diameter and rich in axially aligned keratin microfibrils. Outer cells have multiple laminar layers, 60−600 nm thick and distinctly rich in disulfide bonds. We used an atomic force microscope (AFM) to examine the nanomechanical properties of various structural components using complementary techniques of force-volume imaging and nano-indentation. AFM images of transverse sections of fibers were obtained in ambient environment, and the mechanical properties of several identified regions were examined. The outer cell layer showed a significantly higher mechanical stiffness than the internal cellular core region. Chemical reduction of disulfide bonds eliminated such dichotomy of mechanical strengths, indicating that the higher rigidity of the outer layer is attributed primarily to the presence of extensive disulfide bonding in the exo-cuticle. This is the first detailed correlative study of nano-indentation and regional elasticity measurements in composite biological systems, including mammalian biological fibers.

Keratins[1] are a major structural component of hair fibers and contribute to a range of essential functions, including physical and chemical protection and temperature control (*1*). Keratins are also proposed to provide mechanical strength. Several models exist to correlate mechanical properties with structural features: the keratin intermediate filament proteins are linked with the intrinsic strength and elasticity properties (*2*, *3*) and the keratin associated matrix proteins are linked with lateral mechanical properties (*4*). However, there is a lack of direct supporting experimental data, primarily due to a paucity of techniques for simultaneous examination of microdomain mechanical properties and the underlying ultrastructures.

Ultrastructural studies of hair fibers, including wool, using electron microscopy and histochemical techniques, reveal highly organized subcomponents (*5*, *6*). Wool fibers primarily consist of a core cellular component surrounded by an outer layer with one or two cuticle cells. The core component contains cortical cells arranged in an overlapping and interdigitating fashion and elongated in the direction of the fiber axis. Cortical cells are composed of microfibrils organized into larger aggregates or macrofibrils. These microfibrils contain aggregated keratin intermediate filament proteins, surrounded by keratin-associated matrix proteins containing high levels of sulfur and tyrosine (*7*). Major cortical cell types can be divided into ortho-, para-, and meso-cortical cells with different size and distribution of macrofibrils and different intra-macrofibril organization of the individual microfibrils and associated matrix proteins (*5*).

The cuticle cells have a laminar structure with an outer exo- and inner endo-cuticle layer (*8*). The exo-cuticle contains an A-layer (the outermost layer) and a B-layer. The A-layer is 30−60 nm thick (*9*) with a covalently bound lipid surface coat that provides water repellant properties and is rich in disulfide cross-links due to a cystine content of up to 35% (*8*, *10*) as well as in isopeptide (-amino (-glutamyl) lysine) cross-links (*10*, *11*). The B-layer is considerably thicker (30−600 nm) and is also rich in disulfide cross-links (15% cystine) and isopeptide cross-links (*10*, *11*). In contrast, the endo-cuticle is relatively lightly cross-linked containing ∼3% cystine.

With its well-characterized ultrastructure and chemical features, a wool fiber provides an ideal two component model system to examine the role of various structural and chemical components in providing mechanical strength. Existing theoretical models for the physical properties of wool fibers also suggest that the cortical components (the intermediate filaments in particular) contribute significantly to the lon-

[†] This work was supported by a NZ science and technology fellowship to ANP from the New Zealand Foundation for Science, Research and Technology. NIH (GM-NIA) to RL and WRONZ to WGB.

* To whom correspondence should be addressed. (RL), Telephone: (*805*)-893-2350. Fax: (*805*)-893-2005. E-mail: rlal@physics.ucsb.edu. (AP), Telephone: (+64) 3-325-2421. Fax (+64) 3-325 2717. E-mail: ashok_parbhu@clear.net.nz.

[‡] Wool Research Organization of New Zealand.

[§] Neuroscience Research Institute.

[1] A portion of this article has appeared in abstract form for the American Society for Cell Biologists Annual meeting, 1998.

10.1021/bi990746d CCC: $18.00
Published on Web 08/21/1999

gitudinal tensile strength (*3*), and the cuticle cells contribute to torsional and lateral mechanical properties (*3*). Significantly, there is a lack of direct experimental data supporting these models, primarily due to a paucity of techniques for simultaneous examination of microdomain mechanical properties and the underlying ultrastructures. Atomic force microscopy (AFM)[2] (*12*−*14*) can map elasticity (Young's modulus) (*15*), plastic deformation, and the ultrastructural features with nanometer spatial resolution, using the recently developed "force-volume" (*16*, *17*) and nano-indentation techniques (*18*).

We have imaged with AFM, the ultrastructure of native wool fibers without fixation and staining. Using the "force-volume imaging" and "nano-indentation" techniques, we measured the relative elastic moduli and hardness of various subcellular components of the wool fibers. Results from these complementary studies show that the exo-cuticle is highly rigid and that the cuticle contributes significantly to the bending stiffness of the fibers. Such findings are consistent with the chemical and structural composition of the cuticle. This is the first detailed correlative study of nano-indentation and elasticity measurements in a mammalian biological fiber. Similar studies of nano-mechanical properties would provide a better understanding of the physicochemical properties of a wide variety of composite biological systems.

MATERIALS AND METHODS

Sample Preparation. Romney wool fibers were washed in distilled water to remove surface debris, the natural suint on the fibers acted as a detergent. The sample was then dried, under vacuum, followed by further washing with freshly distilled anhydrous *tert*-butyl alcohol by refluxing in a Soxhlet apparatus to remove remaining unbound surface lipids. The molecular size of the *tert*-butyl alcohol prevents it from entering the dried wool fiber, avoiding removal of internal lipids. The wool fibers were then embedded unstained in LR white resin (*19*). Keratin fibers are composed of high-density protein bundles that are stable, do not require chemical fixation, and there is insignificant impregnation of embedding resin, thus transverse sections of the embedded fiber are representative of the native fiber.

For correlative ultrastructure imaging with transmission electron microscopy (TEM) and AFM, ultrathin transverse sections with gold to silver interference color (approximately 100 nm thick) were cut using a diamond knife on a LBK ultramicrotome. Initial sections collected using a glass knife had a high surface roughness making them unsuitable for analysis by AFM. The sections were mounted on 100 mesh Formvar-coated PELCO copper locator grids where each mesh point is uniquely identified. These grids were used to identify each of the wool fiber sections so that the exact same fiber area could be imaged with TEM and AFM, successively. The mounted sections were sequentially stained with uranyl acetate and lead citrate using a standard protocol (*20*) in order to increase the sample electron density for TEM.

For elasticity measurements and indentation significantly thicker (1 μm), transverse sections were obtained. This is important so as to minimize the influence of the glass substrate on the elasticity measurements of the individual components. The transverse section ensured that individual components were spatially nonoverlapping and thus there was only one component occupying space between the glass and the tip. After the wool fiber was cut into sections, sections were transferred from the knife boat to glass cover slips by a water film on a wire loop. The glass cover slips were glued onto metal AFM disks with a TEM locator grid sandwiched between the cover slip and the metal disk to assist in identifying individual sections. When the water droplet evaporated, the surface tension forces were sufficient to adhere the sections to the glass surface.

Disulfide Bond Reduction. Disulfide bonds (cystine−cystine) were reduced as described by Weigmann (*21*) with slight modifications. Briefly, the mounted fiber sections were treated with (100 μL) 0.1 M dithiothreitol (DTT) solution in 0.1 M TRIS-buffer (pH 7.6) under argon in a glovebag at 20 °C for 30 s. The newly generated sulfhydryl groups were then alkylated by treatment with a small excess (100 μL) of 1 M iodoacetamide (IAM) solution in a 0.5 M TRIS-buffer of pH 7.6 for 30 s. The sections were then rinsed with oxygen-free water to remove excess reagent.

TEM and AFM Imaging. TEM images of the uranyl acetate and lead citrate stained wool fiber sections were collected with a Phillips CM30 electron microscope operating at 80 kV. The same sample areas examined by TEM were then examined by AFM.

The AFM imaging was conducted with a multimode AFM equipped with a J-scanner and a Nanoscope IIIa controller (Digital Instruments, Santa Barbara, CA). The cantilever of the AFM was positioned over the desired sample area using a dissecting microscope equipped with long working distance objective (180× magnification). Imaging was performed using tapping mode in air with 125 μm etched silicon microcantilevers (TESP) (*16*). Cantilever oscillation was set at its resonance frequency (typically 270 kHz) with a driving voltage of around 200 mV. Samples were scanned at a rate of 0.5−1 Hz. Minimal image processing (only off-line flattening) was performed.

Measurement of Elasticity and Indentation. All elasticity measurements and indentations were performed using the same diamond tip cantilever (Digital Instruments, Santa Barbara, CA). The tip was made of a single crystal of natural diamond, bonded with epoxy to the stainless steel cantilever. The spring constant of the cantilever was approximately 100 N/m.

Elasticity measurements and nano-indentations were made using the "force-volume mode" of the nanoscope software (*16*, *17*) on approximately 1 μm thick transverse section of wool fiber such that the exo-cuticles were often flanking the central core region. The force curves were collected at the same maximum cantilever deflection (relative trigger), at each point in a 64 × 64 array with each force curve sampled at 64 points. The deflection trigger point was set depending on if either the elasticity was measured or the sample surface was being indented.

Elasticity. To measure the elasticity, a reference force curve for the cantilever was obtained by measuring the tip deflection on a hard surface, in this case, the glass substrate (*22*). After the reference curve was established, neither the tip nor the position of the laser spot on the cantilever was changed. The nanoscale elasticity map of the substrate was determined from the force applied and the resulting deforma-

[2] Abbreviations: AFM (Atomic force microscopy), TEM (Transmission electron microscopy), DTT (dithiothreitol), IAM (iodoacetamide).

tion of the sample (*15*). The Sneddon theory, which describes an infinitely hard indenter on a flat, deformable substrate, has been employed successfully for this problem (*23*, *24*). The interaction is described by the Sneddon equation

$$F = \frac{4}{3}\sqrt{r}E\Delta z^{3/2} \quad (1)$$

Where F is the force applied, r is the radius of a parabolic tip, E is the sample elasticity, and z is the indentation (elastic deformation) of the sample. The difference between the force curves measured on the hard and soft samples describes the elastic deformation of the sample by the tip loading force (F). The applied force for each deflection can be calculated from the spring (force) constant of the cantilever. Plotting the obtained indentation against the force, F, gives force vs indentation curves. Thus, elasticity (Young's modulus) can be determined from these curves by fitting them to eq 1 (*24*). For these calculations, the end of the tip is assumed to be parabolic with a radius of approximately 50 nm.

Nano-Indentation. Indentations were made on the sample surface by increasing the cantilever sensitivity parameter in the force-volume software mode to 10 times the actual value. This has the same effect as increasing the relative trigger threshold by 10 times, i.e. increasing the applied force by 10 times. Although the cantilever sensitivity is a nonlinear parameter, a linear approximation is assumed over the small cantilever deflections used in these experiments. This adjustment of the cantilever sensitivity meant the nano-indentation measurements were performed in the load range of about 15 μN for 0.25 s.

The dimensions of the indentations in each of the regions were measured from the line plot analysis function of the Nanoscope IIIA data analysis software. The nano-hardness was calculated as the indentation load divided by the projected residual area (*18*). The projected residual area of the indentations was calculated from the height and base of the triangularly shaped indentation, as measured from the height images.

RESULTS

Imaging Ultrastructure. TEM and AFM images of the same transverse sections of the same wool fiber are shown in Figure 1. The AFM images (Figure 1, parts c and e) were collected after the TEM imaging (Figure 1, parts b and d). At smaller scan sizes (higher resolution), AFM images show an excellent correlation with the TEM images (Figure 1, parts d and e). Cellular arrangement of the cuticle (Cu) and cortical cells (Co) and the cell membrane complex (CMC) between these cells (*7*) is clearly evident in both the TEM and AFM images. Interestingly, the features in the TEM image with heavy stain (dark regions, Figure 1d) appear to correlate with many of the higher features on the AFM image (light regions, Figure 1e).

The excellent correlation of the AFM and TEM images allowed the remaining experiments to be performed using only AFM, with the confidence that the fiber structure is accurately identified.

Force Mapping and Elasticity. Figure 2 shows an example of the difference in the elasticity at several cellular regions as determined from the force-mapping and the underlying ultrastructures in a 1 μm thick transverse section of a wool

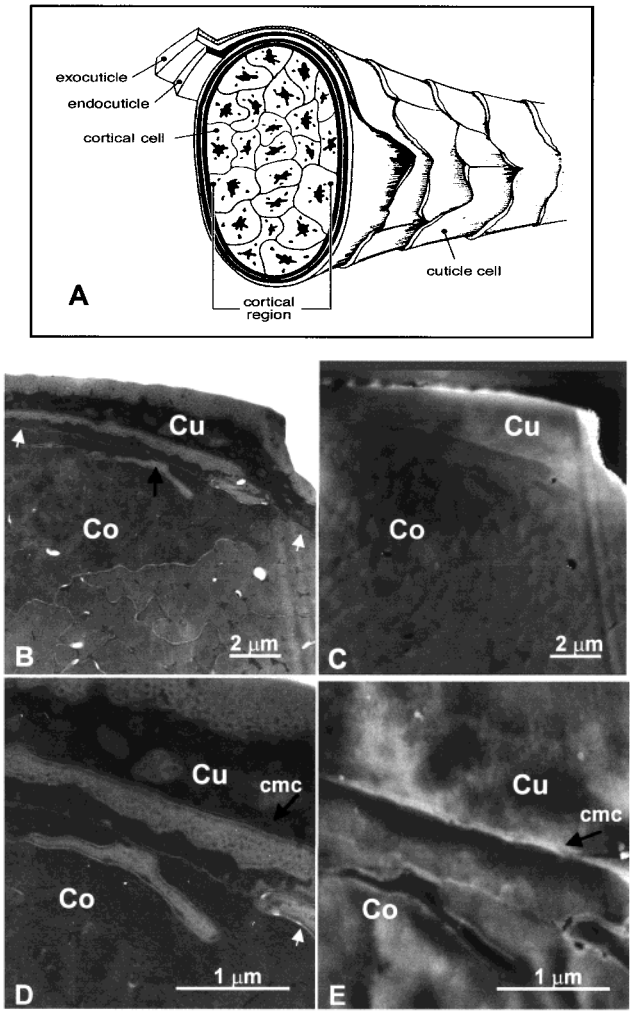

FIGURE 1: (a) Schematic diagram of a wool fiber showing its internal cellular structure, and the cells of the fiber cuticle that form the external layer of the fiber. The model is not to scale and is adapted from Marshall (*7*). (b) A TEM image of the edge of a transverse section of a wool fiber. This image shows two adjacent cuticle cells (Cu) and some portion of the cortical region (Co). The staining pattern shows that the cuticle cells can be further divided into light stained (low cystine) endo-cuticle and dark stained (high cystine) exo-cuticle. The small "finger" like protrusion of cuticle cell into the cortex region of the fiber (black arrow), presumably originates from another cuticle cell, which lay above or below the sectioning plane. The white arrows indicate the demarcation between the cuticle and cortical cells. (c) AFM height image obtained in tapping mode (512 lines at 1 Hz scan rate) of the same wool fiber area as the TEM image in Figure 1b. (d) TEM image of the same wool fiber at higher magnification, this image shows two cuticle cells and a section of the cortex. The cell membrane complex (CMC) is clearly visible in the TEM image as a classic tramline feature between cells. Again, the white arrows indicate the demarcation between the cuticle and cortical cells. (e) AFM height image of the same area as the TEM image in Figure 1d. From this image, similar features to the TEM image are observed. It is interesting to note that the depression (i.e., the lower thickness) in the AFM image (darker regions, Figure 1e) corresponds to less densely stained areas in the TEM (lighter regions, Figure 1d). A comparison of Figure 1, parts b and c shows that at large scan sizes AFM images provide limited information of the subcellular structure in contrast to the TEM images of the wool fiber. The TEM image has a higher lateral resolution than the AFM image, since the AFM images of a larger scan area is limited by the maximum pixel size (512 $\times$ 512 pixels). However, at small scan sizes AFM images correlate well with TEM identified subcellular structures.

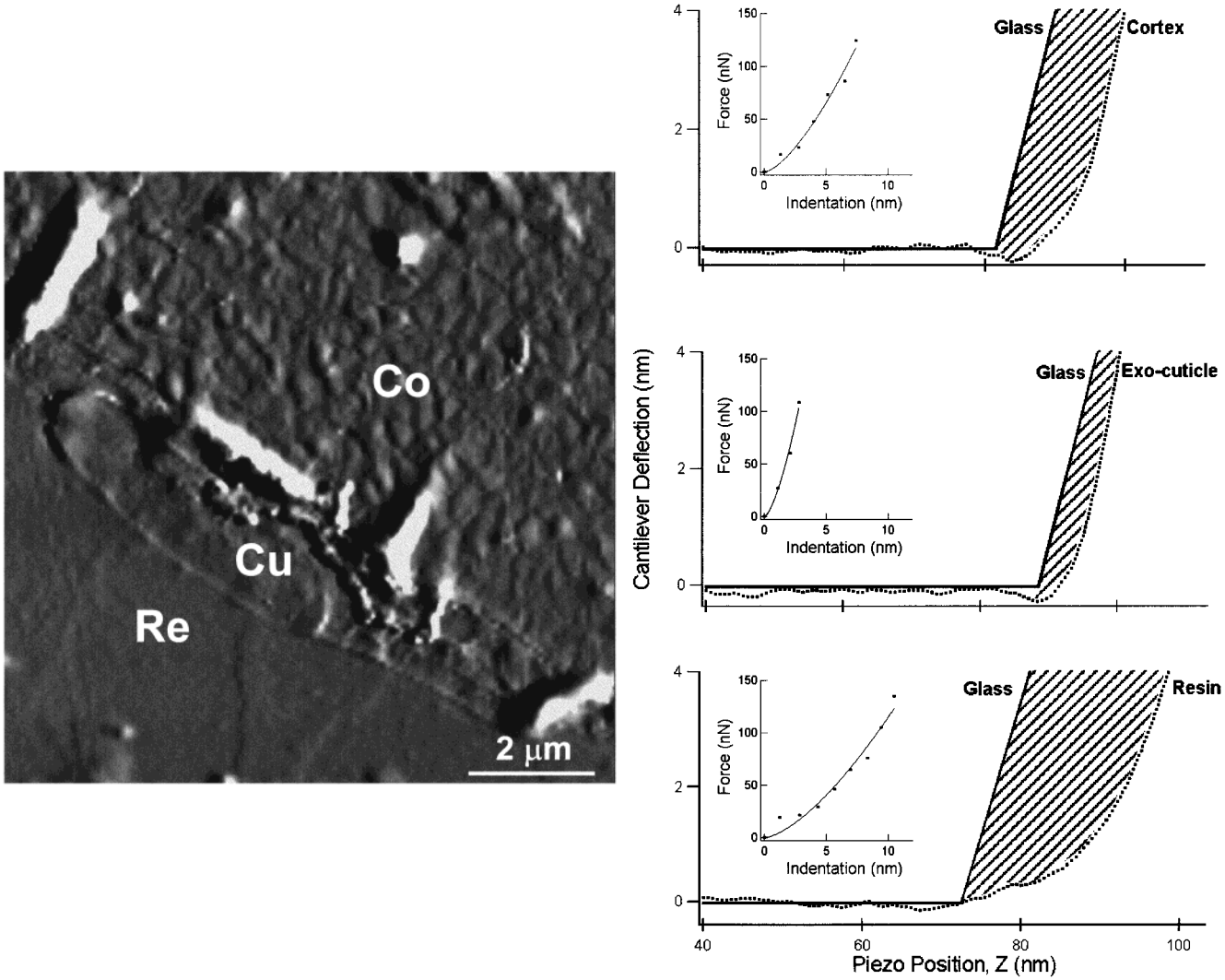

FIGURE 2: AFM imaging of the surface topography and the force-indentation plots. Left panel: an amplitude-mode image of the edge of a transverse-sectioned wool fiber, corresponding to the region whose elasticity was mapped using the force-volume software. The image was taken in tapping mode at 1 Hz and 512 × 512 pixels. The regions shown are the cortex (Co), cuticle (Cu), and embedding resin (Re). This image is presented, as opposed to the height image, from the force-volume map because it has a higher pixel resolution and the amplitude image is approximately the first derivative of the height so it has enhanced contrasted at the edges making it easier to resolve the cellular composition. Typical cantilever deflection vs piezo *z* position for different components of the wool fiber transverse section are plotted in the panels on the right (dotted line). Superimposed on each of these curves is the averaged glass reference deflection curve (solid line), the shaded area between these two curves is representative of the relative elasticity, the larger the area the greater the elasticity. Representative force vs indentation plots of the different components have also been calculated and are displayed as insets next to each deflection plot. The points represent the calculated force vs indentation, while the solid line is the fitted curve used to determine the relative elasticity (equation 1). For a given region, a larger indentation at equivalent force corresponds to components with greater relative elasticity.

fiber. In the topography image (left panel, Figure 2), the cortical region (Co), cuticle cells (Cu), and embedding resin (Re) are identified. The exo-cuticle region was identified at high resolution. The approach components of typical deflection vs *z* position plots for different regions of the fiber are shown in the right panels of Figure 2. From these data, the force vs indentation plots were calculated (*15*) (insets in the right panels of Figure 2). The applied forces were within the elastic limit of the sample. As the same tip was used for each experiment, the force vs indentation plots could be used to determine the relative elasticity for each fiber region using eq 1. Such analysis shows that the Young's modulus of the exo-cuticle is the highest and ~19.8 GPa, while the cortical region and endo-cuticle have significantly lower Young's modulus of 4.0 and 3.8 GPa, respectively (see Table 1). This suggests that the exo-cuticle is the most stiff compared to the cortical and endo-cortical regions.

Table 1: Relative Elasticity and Hardness of a Subcomponent of a Wool Fiber

	Young's modulus of native wool (GPa)	Young's modulus of DTT reduced wool (GPa)	hardness of native wool (GPa)
exo-cuticle	19.8 ± 8.4 (11)	0.35 ± 0.1 (9)	3.9 ± 0.4 (8)
endo-cuticle	3.8 ± 1.5 (9)		2.5 ± 0.2 (4)
cortical	4.0 ± 1.7 (15)	0.48 ± 0.2 (24)	0.9 ± 0.07 (6)
embedding resin	2.6 ± 0.4 (11)	1.1 ± 0.2 (9)	0.9 ± 0.1 (8)

[a] Relative Young's moduli of native and DTT reduced wool fiber components, correlated with relative hardness values of these components calculated from nano-indentations. Numbers of measurements are given in parentheses.

Nano-Indentations. As an independent and complementary measure of the mechanical properties of the fibers, the Nanoscope IIIA force-volume software was used to create plastic deformations at a nanometer scale (nano-indentations) on the

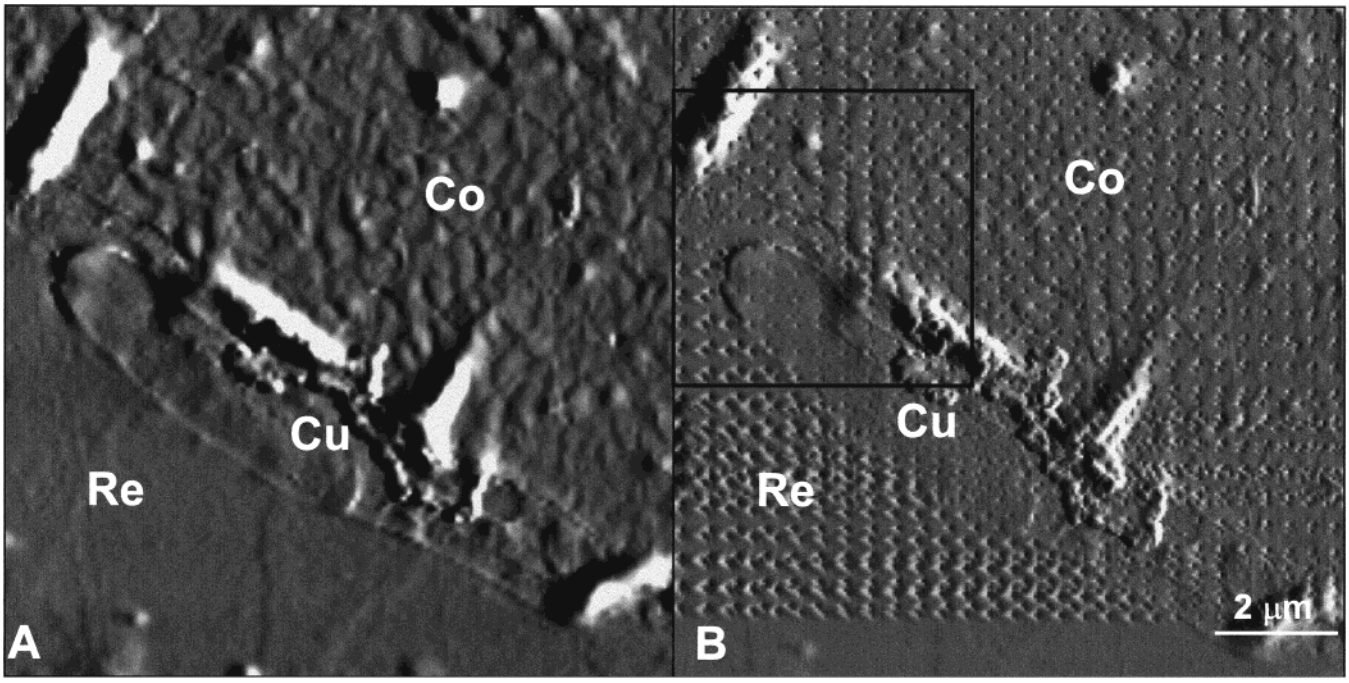

FIGURE 3: AFM amplitude mode images of the edge of the same wool fiber transverse section (512 lines at scan rate of 1 Hz), showing the cortex (Co), cuticle (Cu), and embedding resin (Re) before (3a) and after nano-indentation (3b). There are two sets of indentations in the surface as the force-volume mode contacts the surface in both the trace and retrace of the scan. The box indicates the area scanned in Figure 4.

sample. Because of a considerably higher stiffness of the wool fibers, a diamond tip-cantilever was used for such study and produced considerable indentations at high-loading force (approximately 15 μN). Figure 3 shows amplitude mode images of the surface of a 1 μm thick transverse section of a wool fiber before (Figure 3a) and after nano-indentation (Figure 3b). The image before nano-indentation shows the cuticle cell, cortical cells, and embedding resin. The image after nano-indentation of the same region (as in Figure 3a) shows an array of nano-indentations (shaped as the pyramidal tip) from the force-volume mapping. The indentations are formed in pairs as a consequence of the force-volume software; the indents are created in both the trace and retrace scans. Only the indentations that were made during the trace scan were used in the calculation of the hardness as this was the direction of data acquisition, and thus, the load applied to create the indentations is known.

Figure 4 shows a higher resolution image of the indentations in Figure 3b. The areas of the plastic deformations on the exo-cuticle are significantly smaller than on the endo-cuticle, cortical cells, or the resin.

The nano-hardness was calculated as the indentation load divided by the projected residual area (*18*). The projected residual area of the triangularly shaped indents was calculated from their height and base, which ranged in width from 88 to 182 nm. From these apparent size differences in the nano-indentations, the exo-cuticle appears to be relatively harder than the endo-cuticle, cortex, and resin.

Disulfide Bonds and Their Role in Fiber Stiffness. The greater stiffness of the exo-cuticle, compared to endo-cuticle and cortex, could result from the preponderance of disulfide cross-links and the isopeptide linkages in the exo-cuticle. To investigate the relative contribution that the disulfides have on the exo-cuticle rigidity, the elasticity of a transverse section of wool fibers were measured after reduction of the disulfide linkages. This was achieved by reducing the disulfide bonds with DTT and alkylation of the free thiol (−SH) group with IAM. The resulting elasticity of the exo-cuticle and the cortex are given in Table 1. Significantly, a comparison of the elasticity of the native and reduced wool fibers shows that after the reduction of disulfide bonds the elasticity of the exo-cuticle decreases from 19.8 to 0.35 GPa, and the elasticity of the cortex decreases from 4.0 to 0.48

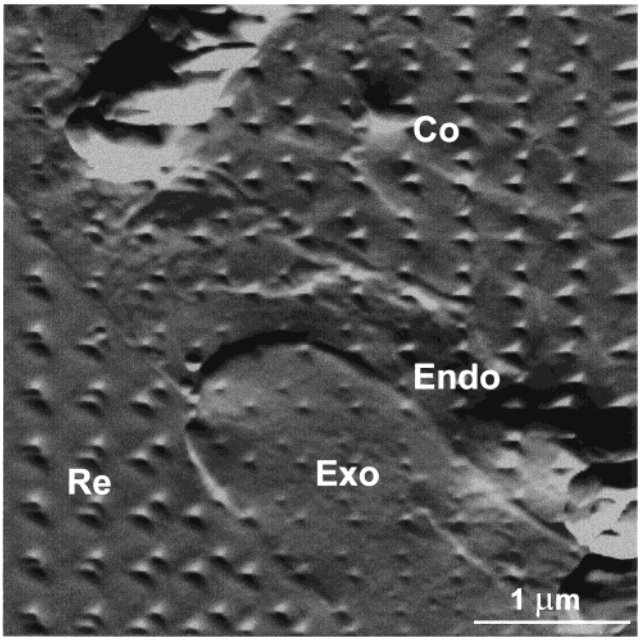

FIGURE 4: AFM amplitude mode image (512 lines at scan rate of 1 Hz) of part of the wool fiber transverse section imaged in Figure 3b at higher resolution to show the shape of the indents made by the diamond tip in the different cell components. The indentations on the exo-cuticle (Exo) are smaller compared to the endo-cuticle (Endo) and cortex (Co), indicating that it is harder.

GPa. Thus, these two structurally different regions have relatively similar elasticity after the removal of disulfide bonds. Elasticity of the endo-cuticle was not measured, because after the reduction of the disulfide bonds, the boundary between the exo- and endo-cuticles could not be determined with any certainty. Significantly, the elasticity of the embedding resin is smaller than the native wool fiber (Table 1). The change in elasticity of the resin component after the reduction of the associated fiber is small. However, the elasticity of the resin is significantly larger than the elasticity of the wool fiber components after the reduction of the disulfide bonds (Table 1).

DISCUSSION

Ultrastructure of native wool fibers was imaged with complementary techniques of AFM and TEM. Both TEM and AFM provide identical ultrastructural information. The "force-volume imaging" and "nano-indentation" features of AFM were used to examine the relative nano-mechanical properties (elasticity and hardness) of various structural subcomponents, including both the cuticular and cortical regions. The outer cuticle layer appears significantly harder than the cortical component: the exo-cuticle is an order of magnitude stiffer than the endo-cuticle and the cortex (Table 1). Chemical reduction of disulfide bonds eliminated such dichotomy of mechanical strengths.

The exo-cuticle is rich in disulfide cross-links (>15% cystine) and ϵ-amino (γ-glutamyl) lysine cross-links. In contrast, the endo-cuticle is relatively lightly cross-linked containing around 3% cystine. The preponderance of disulfide cross-links in the exo-cuticle could account for the higher mechanical stability. Consistent with this possibility, the reduction of disulfide bond cross-links also decreased the stiffness of both the exo-cuticle and the cortex, but the reduction in the elasticity of the exo-cuticle is much greater, resulting in a elasticity value close to that of the cortex (Table 1). The exo-cuticles consist of two layers (A and B). The regional difference in the stiffness of these two layers were not differentiated as the end radius of the diamond tip used in this study was nominally in the size range of the A-layer (30−60 nm). However, as these two layers have a significantly different amount of cystine content, their mechanical properties are expected to differ considerably. This is reflected in the large variance in the elasticity data for the exo-cuticle compared to the other measured regions (see Table 1).

Hydrogen and ionic bonding have also been proposed to contribute to the longitudinal shear modulus of an intact wool fiber (*4*, *25*). However, in the present study, the stiffness was measured on nondehydrated wool fibers at room humidity. We have assumed that small humidity changes would have only a small effect, due to hydrogen and ionic bonding (*4*), on the primary contribution of the disulfide bonds before and after reduction.

In the present models for the strength of wool fibers, the role of the cuticle is considered insignificant and the fiber is treated as a homogeneous system composed exclusively of cortical material. This is based on the idea that the cuticles "slide" over each other during mechanical deformation. As the cuticle cells are developing, the outer cell leaves an impression on the under lying cuticle cell. If the upper cell is removed from, or slides off, the lower cell, then the impression is clearly visible. However, as shown in Figure 5, in a controlled stretching of wool fibers where mild reductive chemistries are employed, the cuticle cells are observed to stretch longitudinally with the cortex stretching considerably rather than sliding apart. Thus, cuticle cells appear to be rigidly fixed.

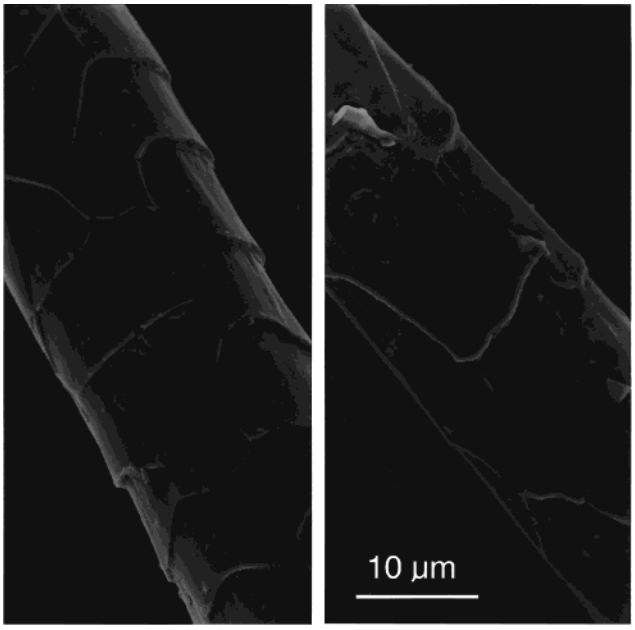

FIGURE 5: Effect of stretch setting on Wool. Scanning electron microscope (SEM) micrograph of (A) untreated wool fiber and (B) Stretch-Set wool fiber. Note lack of imprints on the underlying cuticle show that the cuticle cells have stretched along with the fiber showing minimal slippage, indicating that they are strongly adhered to the underlying cortex.

For a wool fiber of homogeneous composition and circular cross-section, the bending stiffness (K_b) can be expressed as (*26*)

$$K_b = \frac{E\pi r^4}{4} \tag{2}$$

where r is the radius. The derivation of this formula assumes that the fiber has linear elasticity and is bend through a small displacement only. If the exo-cuticle is assumed to be rigidly fixed to the outer layer of the fiber and to be linear elastic, then the contribution of this additional layer with different elastic moduli to the bending stiffness can be expressed as

$$K_b = \frac{\pi}{4}[(E_1 - E_2)r_1^4 + E_2 r_2^4] \tag{3}$$

where E_1 is the elasticity of the cortical material, E_2 the elasticity of the exo-cuticle, r_1 the radius of the cortical region of the fiber, and r_2 the radius of the complete fiber.

The measured relative Young's moduli for the exo-cuticle and the cortical regions of the fiber, when fitted to eq 3, suggest that a fiber with a diameter of 30 μm will be 20% stiffer with a 0.5 μm exo-cuticle layer, compared to a 30 μm fiber without an exo-cuticle. This result suggests that the exo-cuticle contributes a significant portion of the overall fiber flexibility, even though it is a minor component of the wool fiber structure. Modification of the mechanical properties of these layers by decreasing the disulfide cross-link

density may, therefore, have a significant effect on the stiffness of the exo-cuticle and thus alter physical properties of wool fibers. Moreover, the presence of a high degree of intermolecular cross-linking in the exo-cuticle layer suggests that physical properties of the outer cuticle would be similar to those expected of a rigid polymer. This rigidity coupled with the location of the cuticle implies that the exo-cuticle has a dominant influence on fiber bending stiffness properties.

In summary, the nano-mechanical properties have been correlated to subcellular wool fiber regions differing in keratin protein composition using the complementary techniques of "force-volume imaging" and "nano-indentation" paradigms of AFM. The exo-cuticle has a significantly higher mechanical stiffness than the internal cellular components. This rigidity can be attributed primarily to the presence of extensive disulfide bonding in the exo-cuticle. Such high rigidity of the exo-cuticle could, disproportionate to its mass, contribute considerably to the bending stiffness of the fiber. Similar studies of nano-mechanical properties would provide a better understanding of the physicochemical properties of a wide variety of composite biological systems.

ACKNOWLEDGMENT

We thank Drs Nils Almqvist and Arjan Quist for assisting with data analysis and helpful discussion, Dr Wayne Munroe for the mechanical model, Gail Krsinic for the wool stretch set SEM images, and Jeff Elings at Digital Instruments for supplying the diamond tip cantilever. We thank Ken Linberg for assistance with TEM studies and Maura Jess for figure preparation.

REFERENCES

1. Orwin, D. F. G., Woods, J. L., and Ranford, S. L. (1984) *Aust. J. Biol. Sci. 37*, 237−255.
2. Rogers, G. R., Hickford, J. G. H., and Bickerstaffe, R. (1994). *Proc. 5th World congress on genetic applied to livestock production, Guleph, Canada, 21*, 291−294.
3. Wortmann, F. J., and Zahn, H. (1994) *Text Res J 64*, 737−743.
4. Kawabata, S., Niwa, M., Muraki, C., Inoue, M., Uyama, M., and Rengasamy, R. S. (1995). *Proc. 9th international wool and textile research conference, Biella, Italy*, II, 124−142.
5. Rogers, G. E. (1959) *Ann. N. Y. Acad. Sci. 83*, 378−399.
6. Orwin, D. F. G. (1979) *Int. Rev. Cytology 60*, 331−374.
7. Marshall, R. C., Orwin, D. F., and Gillespie, J. M. (1991) *Electron Microsc. Rev. 4*, 47−83.
8. Ruetsch, S. B., and Weigmann, H. D. (1995). *Proc. 9th international Wool textile research conference, Biella, Italy*, II, 45−55.
9. Leeder, J. D. (1986) *Wool Sci. Rev. 63*, 3−35.
10. Swift, J. A. (1997) in *Formation and structure of human hair* (Jollès, P., Zahn, H., and Höcker, H., Eds.) pp 149−175, Birkhäuser Verlag, Basel, Boston.
11. O'connor, S. D., Komisarek, K. L., and Baldeschwieler, J. D. (1995) *J. Invest. Dermatol. 105*, 96−99.
12. Binnig, G., Quate, C. F., and Gerber, C. (1986) *Phys. Rev. Lett. 56*, 930−933.
13. Lal, R., and John, S. A. (1994) *Am. J. Physiol. 256*, C1−C21.
14. Shao, Z. F., Mou, J., Czajkowsky, D. M., Yang, J., and Yuan, J. Y. (1996) *Adv. Phys. 45*, 1−86.
15. Shroff, S. G., Saner, D. R., and Lal, R. (1995) *Am. J. Physiol. 269*, C286−92.
16. Laney, D. E., Garcia, R. A., Parsons, S. M., and Hansma, H. G. (1997) *Biophys. J. 72*, 806−813.
17. Rhee, S. K., Quist, A. P., and Lal, R. (1998) *J. Biol. Chem. 273*, 13379−13382.
18. Bhushan, B., and Koinkar, V. N. (1994) *Appl. Phys. Lett. 64*, 1653−1655.
19. Nelson, W. G., and Woods, J. L. (1996) *J. Microsc-Oxford 181*, 88−90.
20. Hayat, M. A. (1970) *Staining*, Van Nostrand Reinhold Company, New York.
21. Weigmann, H. D. (1968) *J. Polymer. Sci, Part A 6*, 2237.
22. Vanalandingham, M. R., McKnight, S. H., Palmese, G. R., Eduljee, R. F., Gillespie, J. W., and McCulough, R. L. (1997) *J. Mater. Sci. Lett. 16*, 117−119.
23. Sneddon, I. N. (1965) *Int. J. Eng. Sci. 3*, 47−57.
24. Vinckier, A., and Semenza, G. (1998) *FEBS Lett 430*, 12−6.
25. Arai, K., Hirata, T., Nishimura, S., Hirano, M., and Naito, S. (1993) *J. Appl. Polym. Sci. 47*, 1973−1981.
26. Landau, L. D., and Lifshits, E. M. (1970) *Theory of elasticity*, Pergamon Press, Oxford, New York.

BI990746D